Particle-in-cell Monte Carlo modeling of Langmuir probes in an Ar plasma

A. Cenian[a)]
The Szewalski Institute of Fluid-Flow Machinery, Polish Academy of Sciences, 80-952 Gdańsk, Fiszera 14, Poland

A. Chernukho
Heat and Mass Transfer Institute, National Academy of Sciences of Belarus, P. Brovki Street 15, 220072 Minsk, Belarus

A. Bogaerts and R. Gijbels
Department of Chemistry, University of Antwerp, Universiteitsplein 1, B-2610 Antwerp-Wilrijk, Belgium

C. Leys
Department of Applied Physics, Ghent University, Rozier 44, B-9000 Ghent, Belgium

(Received 29 September 2004; accepted 25 April 2005; published online 29 June 2005)

The Langmuir-probe diagnostic of a plasma is studied using a particle-in-cell Monte Carlo model. The electron-density, temperature, and potential profiles are determined for a probe immersed in an Ar plasma. The model is verified using the low-pressure results of Sternovsky *et al.* [J. Appl. Phys. **94**, 1374 (2003)]. It was proved that the ion to electron temperature ratio may not be constant in the sheath–presheath region. © *2005 American Institute of Physics*.
[DOI: 10.1063/1.1938275]

I. INTRODUCTION

The Langmuir probe is a well-established diagnostic tool for a low-pressure, stationary plasma. Most of the analytical probe theories were developed under the assumption of a collisionless probe sheath (ion motion determined by electric field), a Boltzmann electron profile ($n_e(x)=n_{e0}\times\exp[-eU(x)/kT_e]$), and a constant electron to ion temperature ratio, T_e/T_i (see, e.g., Ref. 1). In the case of collisional-probe theories[2,3] diffusion was included into the description of ion motion. The high-pressure theories of electrical probes immersed in a combustion front were modified later[4] in order to include also plasma convection effects, both in the case of thin and thick probes. The values of the probe current, determined using the usual continuum formulas, underestimate the values measured under flowing conditions even by an order of magnitude.[4]

Moreover, even for a plasma of the middle-range pressure ($1<p<10$ mTorr), i.e., in the weakly collisional case, there are various problems to be solved. For instance, the orbit-motion-limited (OML) theories[5] overestimate the densities measured using other techniques (nonprobe) even by an order of magnitude.[6,7] Zakrzewski and Kopiczyński[8] proved already that in the weakly collisional case a single collision, decelerating an ion in a sheath, could increase the ion current of small-diameter probes, whereas multiple collisions lead to a current decrease. Recently, Sternovsky *et al.*[7] and Sternovski and Robertson[9] have proposed a model extending the OML formula by addition of ion current related to slow ions created in charge-exchange processes occurring inside the sheath. The effects of sheath expansion for a thick collisional probe due to ion absorption are also discussed.

Parallel to various analytical models, some numerical models based on the particle-in-cell Monte Carlo (PIC-MC) method (a review of the method could be found, e.g., in the work of Nanbu[10]) have recently been developed for a Langmuir probe.[11–13] Hereafter, we will not go into the details of the PIC-MC method. For more information we encourage reading Ref. 10. Here we will describe only the specific, most important features of the related models.

Kono[11] has proposed a 1d2v [one dimensional (1D) in space displacement, two dimensional (2D) in velocity] PIC-MC model describing a spherical probe immersed in a plasma bulk. The MC trajectories of all charged particles (including electrons), which gradually fill an empty simulation box due to the thermal particle flux from the ambient plasma, are determined. The particles passing through the boundaries of the simulation box are lost (absorbed on the probe surface or into the ambient plasma). All particles move in the electric field generated by the probe bias and the space charge. The collisions are treated in a simplified manner, i.e., the velocity of the colliding particle is replaced by the random thermal velocity corresponding to the temperature of that species and $T^+=T^-=T_e/100$ is assumed, where $T^{+(-)}$ is positive (negative) ion temperature. The stationary particle-density and potential profiles are determined in order to study the process of sheath formation.

Kawamura and Ingold[14] have proposed a 1d3v [1D in space displacement, three dimensional (3D) in velocity] PIC-MC model of an electropositive plasma for cylindrical-symmetry systems. The 3D trajectories are calculated in this model but only the radial (1D) charge distribution is taken into account in Poisson's equation (taking advantage of the assumed symmetry). Both elastic and inelastic (excitation and ionization) collisions of electrons with Ar atoms were considered. Only elastic processes (isotropic and backscattering) were taken into account for the calculation of the ion

a)Electronic mail: cenian@imp.gda.pl

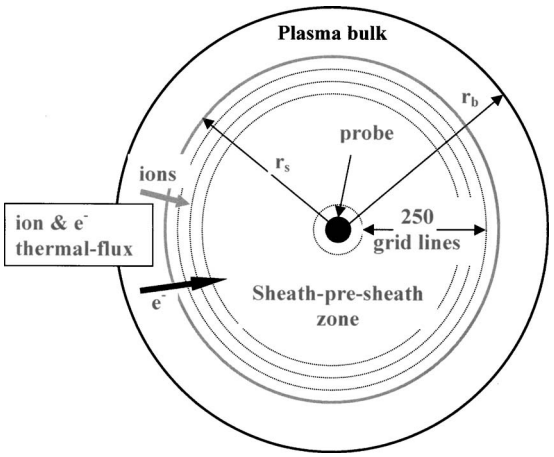

FIG. 1. Scheme of the considered zones in the PIC-MC model; 250 radial grid lines are presented by dotted circles.

trajectories. Preliminary investigations[15] proved already that this type of model could be useful to study some fundamental problems of plasma-wall interactions, including plasma neutrality, the Bohm criterion, and the sheath formation. The above-mentioned models[10,14] served as a background for modeling of cylindrical probes immersed in high- and low-pressure plasma.[12,13] Current–voltage ($I-V$) characteristics of the probes determined using the PIC-MC method were discussed there.

In the presented paper, the PIC-MC model, developed and briefly described by Cenian *et al.*[12,13] for an electrical probe in an Ar plasma, is slightly modified and extended. For instance, the "buffer zone" between the plasma bulk and presheath zone is not considered anymore and a more precise algorithm for the species' orbiting motion in the sheath and absorption on the probe surface is applied. Moreover, in order to verify the model, the results concerning low-pressure ($\sim$0.1 Pa, corresponding to the gas density $n_g \sim 3 \times 10^{19}$ m^{-3}) Ar plasma are compared here with the experimental and other theoretical results of Sternovsky *et al.*[7] Also, the assumptions about the ratio of electron to ion thermal energy ("temperature") and Boltzmann electron profile are discussed.

II. MODEL OF PLASMA-SURFACE INTERACTIONS

The plasma-probe interactions are studied in a system with cylindrical symmetry, related to an infinitely long cylindrical probe, $2r_p$ in diameter, immersed in a continuum, nonflowing, electropositive plasma. The effects of direct current (dc) field sustaining a positive column (directed along the probe symmetry axis) can be taken into account. For the sake of simplification, the whole plasma volume is separated into two different zones: sheath–presheath (SPS) zone and the ring-shaped volume around it (called later the plasma bulk zone) (see Fig. 1). The minimum radius of the SPS zone depends strongly on the probe bias voltage, as will be discussed later. The motion of charged particles in both zones is described by the MC trajectories.

The concentration of charged particles in the plasma bulk is kept constant by assuming that the particles reflect specularly at the boundaries, i.e., at the boundary with the SPS zone and at an external boundary given by r_b (radius of plasma bulk zone). The neutral plasma of the plasma bulk is described by the electron (T_e) and ion (T_i) "effective" temperatures (see Ref. 16). Maxwell distributions were generally assumed as the initial conditions, but other distributions may be easily introduced as well. As the simulations continue, the charged-particle distribution changes drastically (as will be discussed later in the sheath region). Initially, the charged particles are uniformly distributed in the whole considered space, i.e., plasma bulk and SPS zones. Later, the charged-particle densities begin to decay in the close vicinity of the probe, due to the constant flux towards the probe and absorption (followed by recombination) on the probe surface. On the other hand, there is a continuous thermal influx of charged particles from the plasma bulk zone to the SPS zone. This flux is simulated by the creation of a particle entering the SPS zone, with the same velocity as the particle from the plasma bulk zone which was reflected from the border with the SPS zone. When a particle is crossing the same boundary but from the SPS side, it is removed from the simulation.

Hence, the charged particles are specularly reflected at the $r=r_b$ boundary in the bulk plasma zone. Whenever a particle from the bulk plasma zone approaches the $r=r_s$ boundary it is specularly reflected back to the zone but the twin particle continues also its movement in the SPS zone, i.e., an additional particle is generated in that zone. The particles are neglected when approaching the $r=r_s$ boundary from the SPS side. The described procedure allows to keep the charged-particle density (ionization degree) in the plasma bulk zone constant, and it also enables to determine the thermal flux from the plasma bulk to the SPS zone. It was checked that the described procedure is simpler but gives the same results as the one used previously.[13] It should be noted here that the flux from the plasma bulk into the SPS zone is higher than that in the opposite direction, giving a net thermal influx of charged particles to the SPS zone.

The charged-particle MC trajectories in the SPS zone are determined by the Newtonian equations for particle motion in an electric field. It is possible to take into account both the axial field of the dc plasma column as well as the radial field generated by the probe bias and the space-charge density (through the Poisson equation evaluated in 250 grid points) (see Fig. 1). The potential is derived from the integral form of the Poisson equation,

$$E_i S_i = 4\pi \sum_{n=l,i} [Q_{+n} - Q_{-n}],$$

where E_n is the radial field value at the nth grid point, $S_n = 2\pi r_n l$ is the surface of the nth grid element of radius r_n, and $Q_{+n}(Q_{-n})$ is the ion (electron) charge accumulated in the nth grid element. It should be noted that the surface S_n, the charges Q_{+n} and Q_{-n}, as well as other extensive quantities, are calculated per length unit in the model.

The probe surface is assumed to be fully absorptive both for electrons and ions, i.e., a particle is removed from the simulation (absorbed on the probe surface and recombined) when its trajectory passes the probe-wall coordinate (i.e., when $r<r_p$). The difference between the number of absorbed electrons and ions determines the probe current.

The outer radius of the plasma bulk zone r_b is related to the radius of the SPS zone r_s by the relation $r_b=(3/2)^{1/2}r_s$, which ensures that initially in the plasma bulk zone the number of charged particles is ~50% of the number of charged particles in the SPS zone. This can be understood by taking into account the initially uniform spatial distribution of charged particles and by neglecting the volume filled by the probe. Initially, the trajectories of 6000–9000 superparticles in the SPS zone were calculated. Later, this number fluctuates, as some particles are being lost on the SPS borders and others are created, when the charge particles enter the SPS zone as described above. It was found that the ionization processes play only a marginal role in the creation of charged particles in this zone. Each superparticle represents $8\times10^3-1\times10^6$ charged particles per centimeter of probe length, depending on the assumed ion density and SPS radius.

The electrons take part in different collision processes with the target Ar gas atoms, described by cross sections for elastic and excitation processes as well as ionization according to Phelps.[17] The Ar^+/Ar collisions are described by cross sections for elastic collisions: isotropic and backscattering (charge-transfer) processes proposed in Ref. 18. Phelps[18] proposed two different approaches to the description of Ar^+/Ar elastic collisions: (a) based on the isotropic approximation with the momentum-transfer cross section Q_m and (b) based on the partition of cross sections between the isotropic (Q_i) and backscattering-charge-transfer (Q_{ct}) part:

$$Q_m = Q_i + 2Q_{ct}.$$

It has been found (see the Appendix) that the isotropic approximation (a) describes the ion mobility very well but fails to describe properly the ion diffusive motion. Therefore the approximation (b) is used in the probe model.

The Ar gas atoms are assumed to be at rest during the electron/Ar collisions, the so called $T_g=0$ approximation, where T_g is the gas temperature. This is not the case for Ar^+/Ar collisions, because of the much smaller difference between the respective Ar and Ar^+ velocities and the relevance of charge-transfer processes in the SPS region. So, the approximate formula for the ion collision frequency,[19]

$$\nu(u_i) = [(4u_{th}^2/\pi) + u_i^2]^{1/2}/\lambda_{mfp}, \quad (1)$$

is used, which takes into account the thermal speed of Ar atoms $u_{th}=u_{th}(T_g)$, where u_i is the ion velocity and $\lambda_{mfp}=1/[Ar]\sigma$ is the mean free path, [Ar] is the Ar atom concentration, and σ is the total cross section for collision processes with ion participation. This expression describes the increase of collision frequency due to the thermal energy of the target atom, which is especially important for low-energy ions. The results presented in the Appendix show that the $T=0$ K approximation of target atoms leads to a significant increase of mobility as well as diffusivity in the low-E/N region.

The standard null-collision method[20] is applied when calculating MC trajectories. When the decision about the real collision is made, the velocity components of the Ar atom are determined using the rejection method as discussed by Robertson and Sternovsky[19] for the velocity-weighted Maxwellian distribution of Ar atoms. They show that the use of this distribution increases the rate of collisions with high relative velocity and so, decreases the ion mobility [especially at low reduced field (E/N) values] and increases the diffusivity. The determination of target velocity enables to decide (using a random number generator) what type of collision took place (see, e.g., Ref. 21).

III. RESULTS AND DISCUSSION

The above-presented model has been verified using the results of probe measurements in an Ar plasma of a standard double-plasma machine.[7] The experimental results related to several current–voltage characteristics partly presented in Sternovsky *et al.*[7] have been kindly supplied by Sternovsky.[22] Two different cylindrical probes have been used in the experiment, i.e., 94 and 313 μm in radius, both immersed in Ar plasmas under different conditions. Here, we focus mainly on the results related to the thick probe, because in this case the model based on the extended OML formula and collisional term proposed by Sternovsky *et al.*[7] yielded much worse agreement with experimental results. The disagreement was related to sheath expansion in the case when r_p/λ_D reaches 0.5, where λ_D is the Debye length.

A. The probe with $r_p=313$ μm

The first considered case is related to that described by Sternovsky *et al.*[7] in their Fig. 7(a), i.e., a probe in a plasma under the conditions described by the parameters $r_p/\lambda_D \sim 0.26$ and $\lambda_D/\lambda_{mfp}\sim 0.01-0.07$. It means that although the thicker probe ($r_p=313$ μm) is considered, a thin probe approximation ($r_p/\lambda_D<0.5$) in a weakly collisional case can still be applied. The gas pressure measured by Sternovsky *et al.*[7] was 1.3 mTorr and the ions were supposed to be in equilibrium with the gas (room) temperature $T=0.025$ eV, in agreement with some laser-induced flourescence (LIF) measurements in similar plasma devices.[23,24] The charged-particle density (in the bulk plasma zone), $[Ar^+]=7.15\times10^7$ cm^{-3}, was derived by using the Druyvesteyn method as presented by Godyak *et al.*[16] The electron temperature, $T_e=1.9$ eV, was derived from the retarding part of the experimental probe characteristic. Taking into account that $n_g \sim 4.3\times10^{19}$ m^{-3}, the ionization degree $\alpha\sim 2\times10^{-6}$ and $\lambda_D \sim 1.21$ mm under the present conditions.

1. Ion trajectories

In the case of the considered thick probe most of the ions (~70%) move directly to the probe (of which about 20% without any collisions). Only about 30% of the ions pass near the probe surface, moving on some kind of elliptical trajectory. Note that the above numbers may vary with the probe bias and the SPS radius applied. When ions collide with an Ar atom they can "jump" from one quasielliptical trajectory to another one. When the ion velocity after a collision becomes small enough or it is directed to the probe, then the respective ion will be absorbed on the probe. The minimum energy E_{min} for an ion approaching the probe with an impact parameter b, in order to avoid absorption on the probe surface, can be evaluated using the equations of energy and angular momentum conservation,

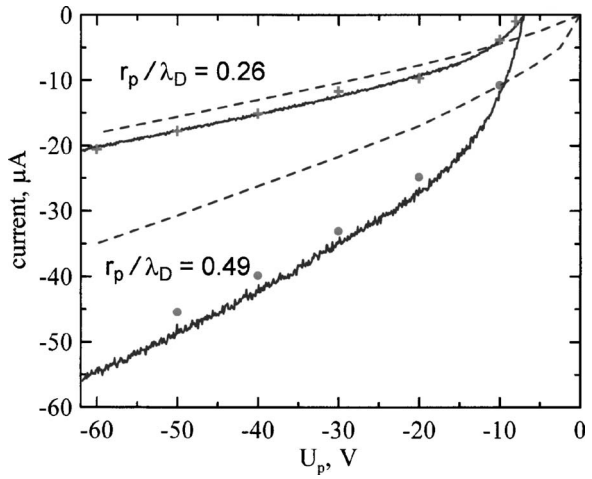

FIG. 2. Characteristic of the 313-μm-thick Langmuir probe in an Ar plasma at p=1.3 mTorr for $[Ar^+]=7.15\times10^7$ cm^{-3}, T_e=1.9 eV, i.e., $r_p/\lambda_D\sim0.26$, and for $[Ar^+]=2.39\times10^7$ cm^{-3}, T_e=1.8 eV, i.e., $r_p/\lambda_D\sim0.49$: (—) experimental results (see Ref. 7) for a plasma characterized by $r_p/\lambda_D\sim0.26$ and 0.49; (---) extended OML theory (see Ref. 7); (+) present results of the PIC-MC model for $r_p/\lambda_D\sim0.26$; (●) present results of the PIC-MC model for $r_p/\lambda_D\sim0.49$.

$$E_{\min} = E(r_p) + |eU_p|,$$

$$E(r_p)r_p^2 = E_{\min}b^2,$$

where $E(r_p)$ is the ion kinetic energy in the close proximity of the probe surface and U_p is the probe potential (see, e.g., Ref. 25). After elimination of $E(r_p)$ one gets

$$E_{\min} = |eU_p|r_p^2/(b^2 - r_p^2).$$

For the probe under consideration and U_p=−50 V it gives 1.25, 0.2, and 0.05 eV for b=2, 5, and 10 mm, respectively. The last value of the impact parameter should be compared with the sheath radius ~8 mm, i.e., even ions with a moderate kinetic energy may leave the sheath probe without being absorbed.

2. Probe characteristic and floating potential

Figure 2 presents the measured ion part of the $I-V$ characteristic (erratic solid lines) compared with the results of the model presented here (symbols) as well as the extended OML model of Sternovsky *et al.*[7] (dashed lines), for two different plasma conditions, which correspond to a ratio r_p/λ_D of 0.26 and 0.49, respectively. Although a relatively good agreement has already been reached between the experimental and model results[7] for a plasma characterized by r_p/λ_D=0.26 [see also his Figs. 6 and 7(a)], the correlation is still improved in the case of the PIC-MC simulations. Moreover, for the plasma characterized by r_p/λ_D=0.49, the agreement with experiment is much better for the PIC-MC results than for the extended OML theory.

According to Sternovsky *et al.*,[7] the growing discrepancy between his theoretical and experimental values when the ratio r_p/λ_D increases is due to the sheath expansion effects. Hence, the good agreement for our calculation results,

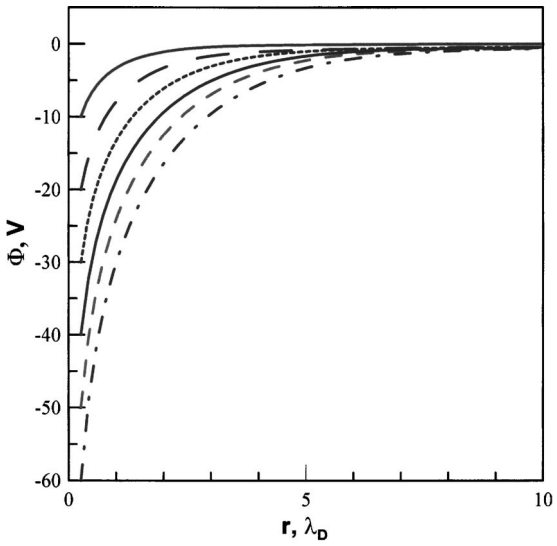

FIG. 3. Calculated potential profiles in the plasma for different probe biases: −10, −20, −30, −40, −50, and −60 V; probe placed in r=0.

observed in the case of the thick probe in Fig. 3, hints that the presented PIC-MC model describes the sheath expansion effects properly.

The observed mismatch between the PIC-MC model and the experimental results for r_p/λ_D=0.49 and high probe biases most probably results from the effects related to the finite length of the cylindrical probe. In order to minimize these effects, long probes, l_p=47 mm in length, were used.[7] The error related to edge effects was estimated, e.g., by Tarrh (1972). The estimation was based on simple expressions derived from the OML theory,[5]

$$i_{+,s} = 1 - ZeU_p/kT_i,$$

$$i_{+,c} = (2/\sqrt{\pi})(1 - ZeU_p/kT_i)^{1/2},$$

for the normalized ion currents to spherical ($i_{+,s}$) and cylindrical probes ($i_{+,c}$), respectively. Here Ze is the ion charge. Assuming that the ion current to the cylindrical probe is given by the sum of the currents to the probe column and a hemispherical tip, Tarrh[26] proposed a relation for the current in the form

$$i_+ = i_{+,c} + c(r_p/l_p)i_{+,s}.$$

From this equation, it can be deduced that for a large probe bias (where the edge effects are most significant) the related error is proportional to the ratio r_p/l_p. Note a linear and a square-root dependence on U_p for spherical and cylindrical probes, respectively. Taking into account that in the considered case $l_p/r_p\sim150$ (and constant $c\sim1$), the error related to the finite length of the probe (edge effects) can become significant only for the highest probe voltages considered, U_p >50 V.

The floating potential V_f, estimated from the calculated characteristic in Fig. 2, is equal to −7.9 V. It agrees quite well with the experimental value[22] of −7.0 V. On the other hand, the values −8.9 and −10.1 V can be derived from the formulas presented in Ref. 27,

$$V_f = -T_e/2[\ln(M/2\pi m_e)], \quad (2)$$

or Ref. 25,

$$V_f = -T_e\left[1 + \tfrac{1}{2}\ln(M/4\pi m_e)\right],$$

respectively, where M/m_e is the ratio of ion to electron mass. A possible source of this discrepancy might be the assumption about the Maxwell energy distributions, used during derivation of the above formulas. It was checked that a multitemperature distribution can be resolved from the experimental characteristics using methods described by Godyak *et al.*[16]

3. Sheath expansion under various probe biases

The relation of the sheath diameter to the Debye length (i.e., with electron density and temperature) is not unique. It was already mentioned that the sheath might expand with increase of the probe radius. It should be added that the sheath and presheath radii increase also with the probe bias voltage. Here, the probe bias, if not otherwise stated, is assumed zero at the plasma potential. Figure 3 presents the calculated spatial profiles of the potential generated in the SPS zone of the investigated probe, for different bias-voltage values, $-60 < U_p < -10$ V. The potential was derived from the integral form of Poisson equation as described in Sec. II. As already mentioned above, the effective diameter of the presheath zone (given by the position where the electric field practically vanishes, $E \sim 0$) increases with the probe bias.

This means that the radius of the SPS zone r_s considered in the model (see Fig. 1) should also increase with voltage. It should be noted also that the ion current of the probe can be limited by the available thermal flux of charged particles. The total ion flux to the probe is proportional to the ion temperature, the surface of the SPS zone, and its radius,

$$\Gamma_+ = eS[\mathrm{Ar}^+]\langle v_i\rangle/4,$$

where the thermal ion velocity $\langle v_i\rangle = (8\ kT_i/\pi M)^{1/2}$ and surface $S = 2\pi l_p r_s$ for a probe of cylindrical symmetry. When the SPS zone radius is too small, the net ion flux into the SPS zone can also be too small in order to provide enough ions. In that case, almost all ions which cross the SPS border are rapidly accelerated and absorbed on the probe surface; hence, the generated space charge is too small. It creates an artificial drop of the plasma potential at the border between the SPS and plasma bulk zone. As an artifact, the flux of ions from the SPS zone to the plasma bulk zone is strongly diminished.

In order to avoid these problems, the ion flux crossing the SPS border from the plasma bulk zone should be significantly larger than the ion current absorbed on the probe surface. In the studied case the critical radius of the SPS zone $r_{\text{s-cr}}$ for which the ion current absorbed by the probe reaches about 95% of its saturation value, was found to be of the orders of 10, 31, and 44 times λ_D, for probe biases of -10, -30, and -50 V, respectively. For the calculation of the current–voltage characteristic from Fig. 2, a value of r_s equal to 18, 40, and 55 times λ_D was used for the respective probe bias. The importance of a proper choice of the SPS radius is clear from Fig. 4, where the calculated ion flux from the plasma bulk zone to the SPS zone (dashed line) and the ion current to the probe (solid line) are presented as a function of r_s, for a probe bias voltage $U_p = -30$ V. The saturation region starting at $r_{\text{s-cr}} \sim 30\lambda_D$ can be observed. At that point, the difference between the ion flux crossing the SPS zone border and probe ion current also starts to become significant. This confirms the estimation of the critical size of the SPS zone.

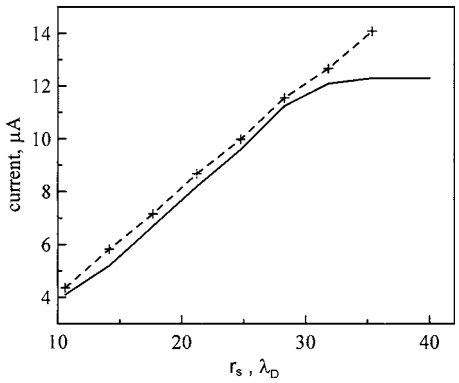

FIG. 4. Calculated ion current to the 313-μm-thick probe (—) and ion flux at the SPS zone border (---) as a function of the SPS radius. The probe bias $U_p = -30$ V.

4. Charged-density profiles

The calculated ion- (dashed lines denoted by "+") and electron-density (solid lines) profiles are presented in Fig. 5. The sheath length — defined by the point where ion and electron densities start to differ significantly — is of the orders of four and nine times λ_D for probe biases of -10 and -60 V, respectively. The significant maximum of ion densities in the sheath region, close to the probe surface, which was absent in the case of our previous simulations[15] is probably related to the change of geometry and orbital motion of ions. In that previous paper, the ion flux to the tube wall was divergent, in contrast to the converging flow to the investigated probe.

The electrons (see the solid lines in Fig. 5) are more and more repelled as they approach the probe vicinity and their

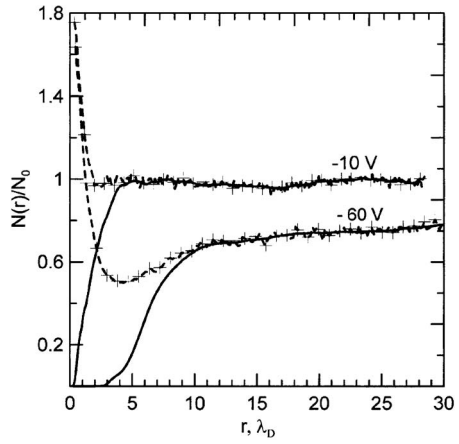

FIG. 5. Calculated density profiles of ions [(---) with (+)] and electrons (—) in Ar plasma for probe biases of -10 and -60 V; $N_0 = [\mathrm{Ar}^+] = 7.15 \times 10^7$ cm^{-3} density of charged particle in bulk plasma. The probe is placed in $r = 0$.

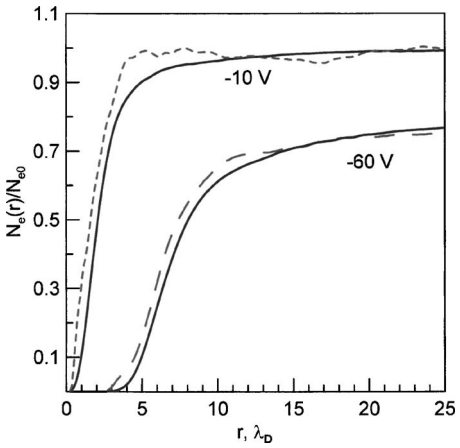

FIG. 6. Comparison of calculated electron (---) and Boltzmann density profiles (—) for probe biases of −10 and −60 V.

density decreases close to the probe surface. At higher probe bias, the density decreases already at larger distances from the probe surface. In Fig. 6 one can see that there is a departure of the calculated electron profile from the Boltzmann profile, $n_e \sim \exp[-eU(r)]$, where $eU(r)$ is the local value of the electric potential. The departure slightly decreases with increase of the probe bias.

5. Thermal-energy profiles

The problems related to the definition of electron- (and even more) ion temperature are well known.[16] For this reason, the notion of "effective temperature" — corresponding to a mean species energy — was introduced. Most of the analytical probe theories use such defined temperatures and assume that the ratio $T_e^{\text{eff}}/T_i^{\text{eff}}$ is constant in the whole plasma volume. However, in the case of the probe-plasma interface, the situation may be much more complicated and deserves another approach.

It should be noted that there is always at least one kind of species attracted to the probe: electrons (and sometimes negative ions) in the case of a positive bias or positive ions in the case of a negative bias. It means that the kinetic energy of such species includes a contribution from the ordered motion (driftlike), and the remaining part is related to a chaotic (thermal) motion. However, an assumed separation may not always be a straightforward action, as can be seen from Fig. 7. The figure presents an attempt to separate the kinetic energy (solid line) in a standard way, i.e., by separation of the ordered (drift) ion motion (dashed line) from the "rest" of the kinetic energy (dotted line) for a bias of −20 V,

$$E_k(r_n) = E_{\text{k-d}}(r_n) + E_{\text{k-rest}}(r_n),$$

where E_k is the ion kinetic energy, $E_{\text{k-d}}(r_n) = m_i\langle dr_n/dt\rangle^2/2$ is a drift energy, and $\langle dr_n/dt\rangle$ is the average (drift) ion velocity in the nth grid element, which has only a radial component due to the symmetry of the considered problem. We consciously avoid describing $E_{\text{k-rest}}$, which strangely enough surpasses the ordered contribution $E_{\text{k-d}}(r_n)$ by far, as energy of a "chaotic" (thermal) motion. The role of ordered motion, which is enhanced by the electric field of the probe, is clearer when looking at Fig. 8, where the ion-speed distributions in

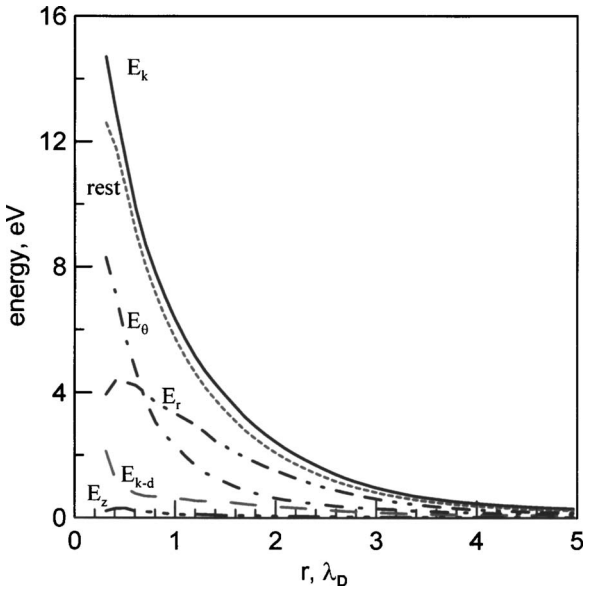

FIG. 7. Calculated kinetic energy of ions and its separation into contributions from driftlike motion in the probe field (– – –) and the rest (-----) for a probe bias of −20 V.

the 5th, 10th, and 15th grid elements for the case of a probe bias of −20 V are shown. The vertical dashed lines represent the velocities corresponding to the electric-field potential in each grid. From the relative positions of distribution maxima with respect to these lines one easily concludes that the ion motion is driven by the electric field and chaotic dynamics plays only a minor role — in contrast to Fig. 7. It should be underlined that any straightforward separation of the rest energy $E_{\text{k-rest}}$ into, e.g., standard radial, azimuthal (tangential), and axial part,

$$E_r = m\langle v_r - \langle dr_n/dt\rangle\rangle^2/2,$$

$$E_\theta = m\langle v_\theta\rangle^2/2,$$

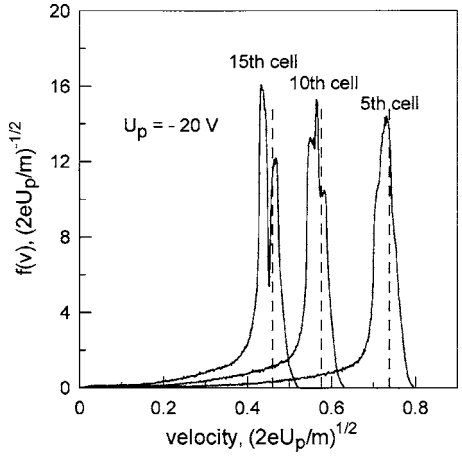

FIG. 8. Calculated ion 2D speed distributions (for the velocity subspace spanned over radial and tangential directions) at the 5th, 10th, and 15th grid elements for a probe bias U_p=−20 V. The velocity is related to that corresponding to the probe-attraction energy eU_p; and the distribution is normalized to 1. The vertical dashed lines represent the velocities corresponding to the electric-field potential in each grid.

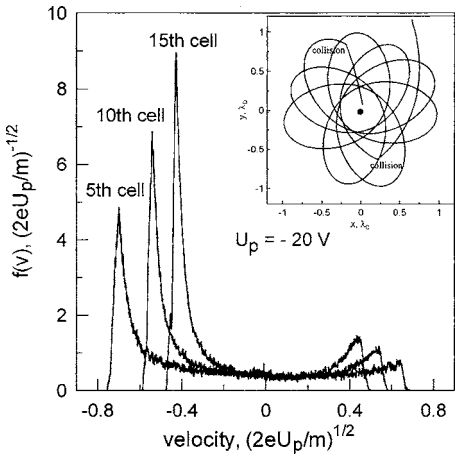

FIG. 9. Ion radial-velocity distribution at the 5th, 10th, and 15th grid elements for a probe bias $U_p=-20$ V. The velocity is related to that corresponding to the probe-attraction energy eU_p, and the distribution is normalized to 1. The exemplary orbital ion-trajectory is presented in the inclusion.

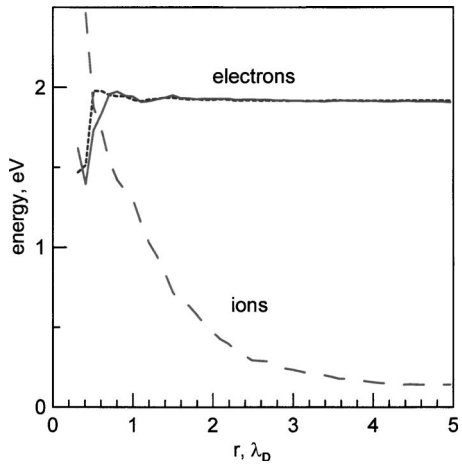

FIG. 10. Calculated ion (– – –) and electron (—) thermal energy profiles. (----) presents the chaotic part of the kinetic energy calculated as subtraction of the drift (ordered) contribution from the total kinetic energy. The probe bias $U_p=-20$ V.

$$E_z = m\langle v_z\rangle^2/2,$$

presented in Fig. 7 as dashed-dotted lines, does not solve the problem.

In order to explain such a small contribution of the drift (ordered motion) to the ion kinetic energy one should consider the influence of the orbital motion of ions. This can be seen in Fig. 9, where the ion radial-velocity distribution is presented for a probe bias of −20 V in the 5th, 10th, and 15th grid elements. The maxima on the left and right sides of the figure correspond to the ions being accelerated by the field towards the probe and those decelerated by the field as they move away from it, respectively. The contribution from the second group of ions leads to substantial reduction of the radial "drift" of ions. However, the orbital motion of ions (with similar velocities — so, orbits) could hardly be assigned as chaotic. Moreover, the chaotic contribution to the ion motion, represented by the rather small width of the distributions in Fig. 8, should be related to collisions and different initial conditions for ions entering the SPS zone.

Before the chaotic contribution to kinetic energy could be properly extracted one should point to the separation of 3D space into the 2D subspace (spanned over radial and tangential directions) and the 1D (axial direction) subspace. It can be seen that the axial part of kinetic energy E_z is even more than one order of magnitude smaller than E_θ and E_r. As the probe field in the axial direction vanishes (except at the probe tip) one can assume that the ion kinetic energy in that 1D subspace corresponds strictly to chaotic (thermal) motion.

Moreover, due to symmetry reasons, there is a strong coupling between ion motions in the radial and tangential directions. As the ion, which passes by, approaches the probe vicinity, its kinetic energy in the tangential direction increases at the expense of the radial one — see E_θ and E_r in Fig. 7. So, a kinetic-energy separation into an ordered and chaotic part in the 2D subspace spanned on the radial and tangential directions should be based on the variance of the speed distribution, $\langle(c-\langle c\rangle)^2\rangle$, somehow related to the chaotic (thermal) energy. The proposed method should be consistent with other cases, e.g., equilibrium with the standard, Maxwell velocity distribution (in 2D),

$$F(c)dc = m/kTc\,\exp[-mc^2/2kT],$$

where c is the 2D speed, i.e., $c^2=v_r^2+v_\theta^2$. Taking into account that the variance $\langle(c-\langle c\rangle)^2\rangle=\langle c^2\rangle-\langle c\rangle^2$, where the average speed, $\langle c\rangle=(\pi kT/2m)^{1/2}$, and the square of the root-mean-square speed, $\langle c^2\rangle=2kT/m$, in the case of a Maxwell 2D velocity distribution, one gets

$$E_{\rm th}^{\rm 2D} = kT = m\langle(c-\langle c\rangle)^2\rangle/(2-\pi/2).$$

The profiles of ion (dashed line) and electron (solid line) thermal energies defined by the above-presented formula are shown in Fig. 10. The results illustrate that the ratio T_e/T_i cannot be considered constant in the plasma sheath region (for radius $r<4\ \lambda_D$ around the probe). Moreover, the ion and electron thermal energies (effective temperatures) become comparable in this region. This is far from our intuitive expectation that the electron temperature is much larger than the ion temperature ($T_e/T_i \gg 1$). The presented conclusions are reinforced by the comparison of the electron thermal energy calculated using the above formula with the chaotic part of the electron kinetic energy in the 2D plane perpendicular to the z axis (see the small dashed line). The good agreement between both values confirms the proposed procedure of thermal-energy estimation. It should be noticed here that the drift (ordered) contribution to the kinetic energy of electrons is not significant as long as the electrons are retarded by the probe field (here it is much less than 0.01% of the electron kinetic energy).

B. The probe with $r_p=94\ \mu$m

In the case of the thin probe, $r_p=94\ \mu$m, the ion trajectories and other characteristics change significantly. The probe characteristics of this thinner probe were investigated under conditions described by the plasma parameters: $p=1$ mTorr, $[Ar^+]=2.43\times10^7$ cm^{-3}, $T_e=1.4$ eV, and $\lambda_D=1.78$ mm, i.e., $r_p/\lambda_D\sim0.053$. A significant difference with

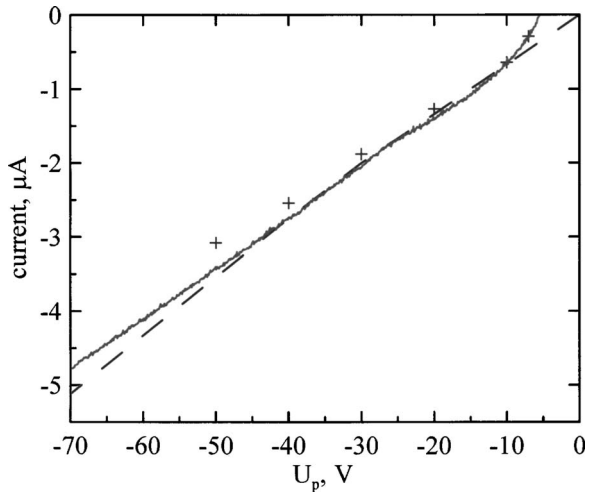

FIG. 11. Characteristic of the thinner Langmuir probe (94 μm) in an Ar plasma at $p=1$ mTorr for $[Ar^+]=2.43\times10^7$ cm^{-3}, $T_e=1.4$ eV, i.e., $r_p/\lambda_D \sim 0.053$: (—) experimental results (see Ref. 7) (---) extended OML theory (see Ref. 7) [presented in his paper in Fig. 6(a)]; (+) present results of the PIC-MC model.

the trajectories for the thick probe has been observed, i.e., ions may perform many more orbits around the probe before they are absorbed on the surface. Even when an ion collides with an Ar atom, it looses some part of its kinetic energy but still not enough to be directly absorbed on the probe surface. Therefore, it performs a few orbits in the probe vicinity before the next collision occurs and the ion is directed to the probe. The number of such orbits can be significant (see inclusion in Fig. 11). In relation to the thick probe much more trajectories are of this type (65% or more). Less than 35% of the ions fall directly on the probe and most of them do it without any collision.

1. Probe characteristic and floating potential

Figure 11 shows the $I-V$ characteristic of the thinner probe, which was applied under the plasma conditions described by the ratio $r_p/\lambda_D \sim 0.053$. The agreement of the PIC-MC results (depicted by the symbol +) with the experiment is here slightly worse than the excellent agreement of the extended OML theory,[7] at least for higher probe biases. This can be explained in the following way. As the average ion velocity increases with U_p some of the considered ions may miss the probe when the time step of the PIC-MC method is too large. On the other hand, by decreasing the time step, one increases the accumulative error of a simulation. Therefore, a reasonable compromise should be met. Another possible source of error may be related to uncertainty in cross sections for electron and ion collisions (some discrepancies between theoretical and experimental drift velocities and characteristic energies can be seen in Figs. 13 and 14). It should be mentioned, however, that the PIC-MC results yield better agreement with experiment than the extended OML theory for very small values of U_p.

The PIC-MC value for the floating potential, ~6 V, agrees reasonably well with the experimental value[7] of ~5.5 V and the value of 6.6 V calculated from formula (2).

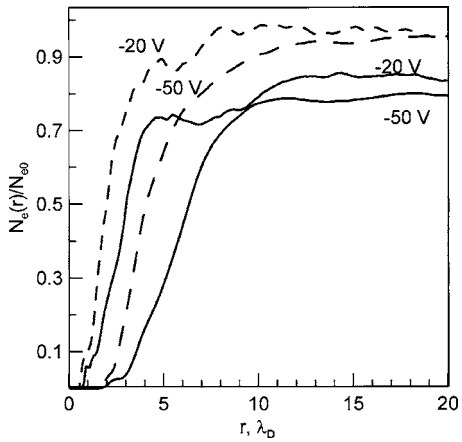

FIG. 12. Comparison of the calculated electron-density profiles for the probe of 313 μm [$r_p/\lambda_D \sim 0.26$ (—)] and 94 μm [$r_p/\lambda_D \sim 0.053$ (---)] for probe biases of −20 and −50 V.

C. Comparison of the calculated spatial profiles for both probes

It was checked that the gradient of the potential in the plasma sheath is much larger in the case of the small-diameter probe ($r_p/\lambda_D \sim 0.053$). This directly influences the electron-density profiles (see Fig. 12). This is expected, taking into account that the Boltzmann spatial profiles describe the electron densities rather well, as was already discussed in relation to Fig. 6.

IV. CONCLUSIONS

It was shown that the discussed PIC-MC model describes reasonably well the experimental $I-V$ characteristics of the probes used by Sternovsky *et al.*[7] It should be stressed that the achieved agreement was better than 11% in the case of the thin-diameter probe ($r_p/\lambda_D \sim 0.053$) and 8% in the case of the thicker probe ($r_p/\lambda_D \sim 0.26$ and 0.49). It should be noted that in contrast to the extended OML theory, the agreement between the PIC-MC and experimental results is better in the case of the thicker probe. It was confirmed that the electron densities are well described by the Boltzmann spatial profile in the considered low-pressure range of plasma.

Moreover, it has been shown that the standard assumption about the constant ratio of electron to ion temperature (besides the problems with temperature definition) could hardly be applied in the sheath region. The ion thermal energy in that region rises (for negative bias) even above the electron thermal energy. A procedure for the ion thermal-energy determination was proposed and verified by the electron thermal energies determined in various ways.

The cross-section sets for ion collision processes were verified by comparison of the respective drift velocities and diffusion coefficients. The use of the elastic cross-section partition into isotropic and charge-transfer parts as proposed by Phelps (1994) was proven to be correct (see the Appendix).

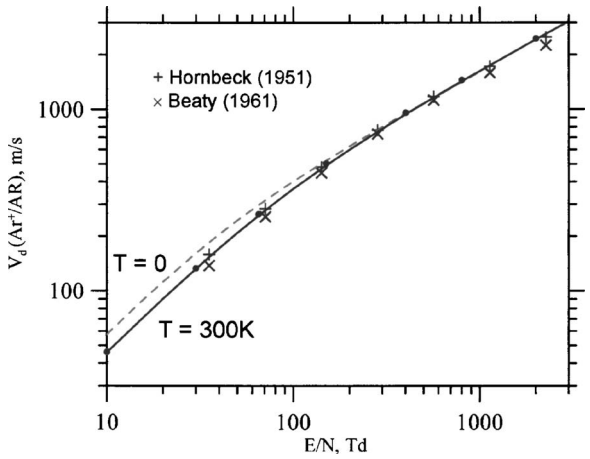

FIG. 13. Drift velocity as a function of E/N for $^{40}Ar^+$ ions in argon: (×) experimental results (see Ref. 34), (+) experimental results (see Ref. 35) (—) present MC results for the model including the effect of isotropic and charge-transfer collisions (Q_i+Q_{ct}), gas thermal motion with $T=300$ K, and velocity-weighted Maxwellian distribution, (●) the same as above but only with isotropic collisions described by Q_m, (----) the same Q_i+Q_{ct} cross sections but with $T=0$ K approximation.

ACKNOWLEDGMENTS

We acknowledge the support of Dr. Z. Sternovsky, who kindly supplied us with related experimental data. The work was sponsored by the bilateral Belgian–Polish cooperation program and the 4T10B 01922 Project of the Polish Committee for Scientific Researches.

APPENDIX

Here, the applied cross-section sets for Ar^+/Ar elastic collisions are verified using the described MC model and experimental swarm data (see Figs. 13 and 14). The cross-section sets for ion collisions[18] have already been partly verified by Jovanović *et al.*,[28] Robertson and Sternovsky,[19] and Piscitelli *et al.*[21] by using different theoretical models. Jovanović *et al.*[28] have shown that the drift velocity calculated using the momentum-transfer theory agrees well with experimental data.[29,30] However, the agreement is slightly worse for the characteristic energy D_T/μ at higher E/N values. Good agreement for the mobility was also confirmed by MC calculations.[19,21] But again, a problem has appeared in the case of the characteristic energy. Robertson and Sternovsky[19] have obtained too low values (in comparison to the experiment[31]), suggesting that the isotropic term of the cross section[18] should be increased significantly. It should be noted that this suggestion contradicts the result.[28] Therefore, we have repeated the swarm calculations, using a model similar to that of Robertson and Sternovsky,[19] but the results are compared with the more recent experimental values.[32] The latter experimental results are systematically lower than those of Sejkora[31] and Schiestl *et al.*[33] According to Stefansson and Skullerud,[32] this might be caused by an uncorrected boundary effect in the fixed-length drift tube used in the former experiments.

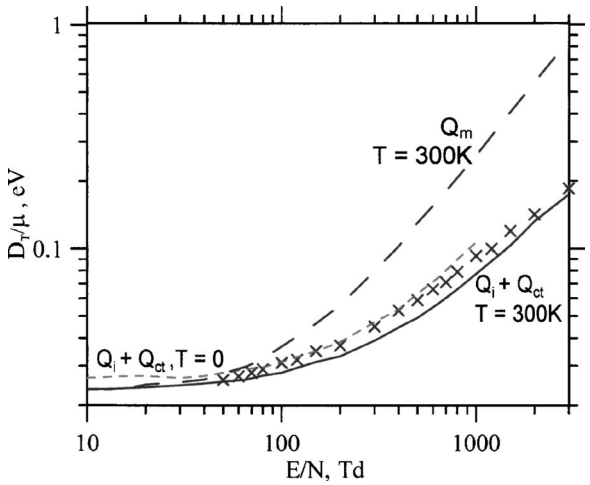

FIG. 14. Characteristic energy as a function of E/N for $^{40}Ar^+$ ions in argon: (×) experimental results (see Ref. 32) (—) present MC results for the model including the effect of isotropic and charge-transfer collisions (Q_i+Q_{ct}), gas thermal motion with $T=300$ K, and velocity-weighted Maxwellian distribution, (— —) the same as above but only with isotropic collisions described by Q_m, (----) the same Q_i+Q_{ct} cross sections but with $T=0$ K approximation.

In order to check the influence of various approximations, three different cases will be discussed:

(i) the present MC model including the effect of cross-section partition into an isotropic and a charge-transfer part (Q_i+Q_{ct}) with gas thermal motion $T=300$ K and velocity-weighted Maxwellian distribution (solid lines in Figs. 13 and 14);
(ii) the same model as above but with the ion collisions in the isotropic approximation described by the momentum-transfer cross sections Q_m (dashed lines and big dots in Figs. 13 and 14); and
(iii) the same Q_i+Q_{ct} partition of the cross sections as in (i) but with $T=0$ K approximation (small dashed lines in Figs. 13 and 14).

Our calculations [model (i)] have confirmed a good agreement with the experimental drift velocity in the case when the effect of gas temperature and velocity-weighted Maxwellian distribution of Ar atoms is included (see the solid line in Fig. 13). The very good agreement with the results[19] should be mentioned. Almost the same values are received using the momentum-transfer cross section Q_m in the isotropic approximation [model (ii)]. However, when the approximation $T=0$ K [model (iii)] is applied for Ar gas atoms, the agreement with the other theoretical and experimental results is a bit worse (at least in the low-E/N range). This exemplifies the influence of gas temperature on the ion motion (significant only for the low-E/N values). In relation to the probe theory it should be noted that the decrease of ion mobility and increase of collision frequency might influence (increase) the ion current to the probe.

The situation is different for the characteristic energy D_T/μ (see Fig. 14). Taking into account that the experimental error[32] is ~4%, our results (solid line) are slightly lower than the experimental values for $150<E/N<1200$ Td (1 Td$=10^{-17}$ V cm^2). However, in the low-E/N region important for the Langmuir-probe calculations the agreement is satisfactory. It should be added here that, although Robertson and Sternovsky[19] claimed a large disagreement, their results (not shown) are only slightly lower than the solid line [model

(i)]. They probably were not aware of the experimental data.[32] When the isotropic momentum-transfer cross-section model is used (Q_m, with $T=300$ K; dashed line), the ratio D_T/μ increases up to four times. When the $T=0$ K approximation for Ar gas atoms is used [model (iii)] (small dashed line) the results are good in the $150<E/N<1200$ Td region but they are too high in the low- and high-E/N regions.

We may conclude that the cross-section set[18] used in the model including the effect of gas thermal motion and velocity-weighted Maxwellian distribution describes the ion motion reasonably well. The $T=0$ K approximation of target atoms leads to a significant increase of the mobility and diffusivity in the low-E/N region. The isotropic [model (ii)] approximation describes the ion mobility very well but fails when diffusive motion is considered.

[1]H. Mott and I. Langmuir, Phys. Rev. **28**, 727 (1926).
[2]C. H. Su and S. H. Lam, Phys. Fluids **6**, 1479 (1963).
[3]I. M. Cohen, Phys. Fluids **6**, 1479 (1963).
[4]R. M. Clements and P. R. Smy, J. Appl. Phys. **40**, 4553 (1969); **41**, 3745 (1970).
[5]See National Technical Information Service Document No. AD 634596 (Institute for Aerospace Report No. 100 by J. G. Laframboise, 1966). Copies may be ordered from the National Technical Information Service, Springfield, VA.
[6]I. D. Sudit and R. C. Woods, J. Appl. Phys. **76**, 4488 (1994).
[7]Z. Sternovsky, S. Robertson, and M. Lampe, J. Appl. Phys. **94**, 1374 (2003).
[8]Z. Zakrzewski and T. Kopiczyński, Plasma Phys. **16**, 1195 (1974).
[9]Z. Sternovsky and S. Robertson, Appl. Phys. Lett. **81**, 1961 (2002).
[10]K. Nanbu, IEEE Trans. Plasma Sci. **28**, 971 (2000).
[11]A. Kono, J. Phys. D **34**, 1083 (2001).
[12]A. Cenian, A. Chernukho, A. Bogaerts, R. Gijbels, and C. Leys, CAPPSA 2004, Proceedings of the International Workshop on Cold Atmospheric Pressure Plasmas: Sources and Applications, Ghent, Belgium, 14–16 January 2004 (University of Ghent, Ghent, Belgium, 2004), pp. 61–64.
[13]A. Cenian, A. Chernukho, A. Bogaerts, and C. Leys, Khim. Fiz. **23**, 3 (2004).
[14]E. Kawamura and J. H. Ingold, J. Phys. D **34**, 3150 (2001).
[15]A. Cenian, A. Chernukho, and C. Leys, Radiat. Phys. Chem. **68**, 109 (2003).
[16]V. A. Godyak, R. B. Piejak, and B. M. Alexandrovich, J. Appl. Phys. **73**, 3657 (1993).
[17]A. V. Phelps, the cross section (10/15/97) available on ftp://jila.colorado.edu/collisiondata/electronneutral/electron.txt (1997).
[18]A. V. Phelps, J. Appl. Phys. **76**, 747 (1994).
[19]S. Robertson and Z. Sternovsky, Phys. Rev. E **67**, 046405 (2003).
[20]H. R. Skullerud, J. Appl. Phys., J. Phys. D **1**, 1567 (1968).
[21]D. Piscitelli, A. V. Phelps, J. de Urquijo, E. Basurto, and L. C. Pitchford, Phys. Rev. E **68**, 046408 (2003).
[22]Z. Sternovsky (private communication).
[23]M. J. Goeckner, J. Goree, and T. E. Sheridan, Phys. Fluids B **3**, 2913 (1991).
[24]G. Bachet, L. Chérigier, M. Carrère, and F. Doveil, Phys. Fluids B **5**, 3097 (1993).
[25]J. P. Raiser, *Fizika Gazovovo Razriada* (Nauka, Moscow, 1987).
[26]S. M. Tarrh, M.S. thesis, Massachusetts Institute of Technology, 1972; cited by E. F. Jaeger, L. A. Berry, and D. B. Batchelor, J. Appl. Phys. **69**, 6918 (1991).
[27]M. A. Lieberman and A. J. Lichtenberg, in *Principles of Plasma Discharges and Materials Processing* (Wiley-Interscience, New York, 1994).
[28]J. V. Jovanović, S. B. Vrhovac, and Z. L. Petrović, Eur. Phys. J. D **21**, 335 (2002).
[29]H. W. Ellis, R. Y. Pai, E. W. McDaniel, E. A. Mason, and L. A. Viehland, At. Data Nucl. Data Tables **17**, 177 (1976).
[30]R. Hegerberg, M. T. Elford, and H. R. Skullerud, J. Phys. B **15**, 797 (1982).
[31]G. Sejkora, P. Girstmair, H. C. Bryant, and T. D. Märk, Phys. Rev. A **29**, 3379 (1984).
[32]T. Stefansson and H. R. Skullerud, J. Phys. B **32**, 1057 (1999).
[33]B. Schiestl, W. Sejkora, M. Lezius, M. Foltin, P. Scheier, and T. D. Märk, in *8th International Seminar on Electron and Ion Swarm* (University of Trondheim, Norwegian Institute of Technology, Trondheim, Norway, 1993), p. 65.
[34]E. C. Beaty, in *Ionization Phenomena in Gases*, Proceedings of the Fifth International Conference (North-Holland, Amsterdam, 1961); quoted in Ref. 19.
[35]J. A. Hornbeck, Phys. Rev. **84**, 615 (1951).